Available online at www.sciencedirect.com
ScienceDirect
Journal of Power Sources 172 (2007) 446–450
JOURNAL OF POWER SOURCES
www.elsevier.com/locate/jpowsour

Short communication

Hydrogen-induced phase transitions in RNi_3 and RY_2Ni_9 (R = La, Ce) compounds

Jing Zhang [a], Fang Fang [a], Shiyou Zheng [a], Jian Zhu [a], Guorong Chen [a], Dalin Sun [a,*], M. Latroche [b], A. Percheron-Guégan [b]

[a] *Department of Materials Science, Fudan University, 220 Handan Road, Shanghai 200433, China*
[b] *Chimie Métallurgique des Terres Rares, UMR 7182, ICMPE, CNRS, 2 rue Henri Dunant, Thiais Cedex 94320, France*

Received 19 May 2007; received in revised form 17 July 2007; accepted 24 July 2007
Available online 28 July 2007

Abstract

Structure stability of RNi_3 and RY_2Ni_9 (R = La, Ce) during cycling of hydrogen absorption/desorption was investigated by both solid-H_2 reaction and electrochemical measurements, in order to understand the mechanism responsible for the poor reversibility, and to reveal the differences between RNi_3 and RY_2Ni_9 compounds. It has been found that, all of the cycled RNi_3 and RY_2Ni_9 were subject to partial amorphization. This hydrogen-induced amorphization (HIA) occurred immediately in $LaNi_3$, but proceeded gradually in $CeNi_3$, LaY_2Ni_9 and CeY_2Ni_9. The HIA in these compounds is attributed to the RM_2 subunits in their crystal structures.

Keywords: Intermetallic compounds; Solid-H_2 reaction; Hydrogen; Amorphization

1. Introduction

Intermetallic RM_3 (R = rare earth, M = transition metal) compounds crystallize either in the rhombohedral structure of $PuNi_3$-type (space group $R{-}3m$) [1] or in the hexagonal one of $CeNi_3$-type (space group $P6_3/mmc$). The RM_3 crystal structure can be regarded as an intergrowth between the RM_5 and the RM_2 subunits, according to the scheme: $RM_5 + 2RM_2 = 3RM_3$ [2]. As a consequence, RM_3 compound could be more receptive to hydrogen than its RM_5 counterpart, because the RM_2 subunit has a higher capacity than the RM_5 subunit theoretically [3]. For instance, the absorbed hydrogen by $LaNi_3$ is 1.54 wt% (at T = 10–40 °C and P = 3.3 MPa), corresponding to an equivalent electrochemical capacity of 411 mAh g^{-1}. However, the stored hydrogen by $LaNi_3$ can only be released partly, which is briefly attributed to the formation of irreversibly amorphous hydrides [4–6].

To overcome this problem, recent interest has shifted to RM_3-based pseudo-binary and ternary compounds, such as RY_2Ni_9 (R = La, Ce). These compounds adopt the same $PuNi_3$-type rhombohedral structure as $LaNi_3$ does, but exhibit higher discharge capacities than the binary compounds [7]. Unfortunately, we have recently found that the complete reversibility of RY_2Ni_9 hydrides is difficult to achieve, especially when charged/discharged at a current density higher than 15 mA g^{-1}. In order to understand the fundamental reason responsible for this finding, and to reveal the differences between the binary and ternary RM_3 compounds, the structural stability of RNi_3 and RY_2Ni_9 (R = La, Ce) after cycling under solid-H_2 reaction and electrochemically charging/discharging were carefully examined in the present study.

2. Experimental

2.1. Sample preparation

Four samples with nominal compositions, $LaNi_3$, $CeNi_3$, LaY_2Ni_9 and CeY_2Ni_9, were prepared by induction melting, followed by annealing at 600 °C for $LaNi_3$ and $CeNi_3$, and 750 °C for LaY_2Ni_9 and CeY_2Ni_9. X-ray diffraction (XRD) was performed at room temperature on a Bruker AXS D8 diffractometer using Cu Kα radiation with a step size of 0.02°. The diffraction patterns were further analyzed by the Rietveld method imple-

* Corresponding author. Tel.: +86 21 65642873; fax: +86 21 65642873.
E-mail address: dlsun@fudan.edu.cn (D. Sun).

0378-7753/$ – see front matter © 2007 Elsevier B.V. All rights reserved.
doi:10.1016/j.jpowsour.2007.07.043

Table 1
Unit cell parameters of the as-prepared RNi_3 and RY_2Ni_9 (R = La, Ce)

Samples	Space group	Lattice parameters (Å)	Cell volume (Å^3)
$LaNi_3$	$R-3m$	$a = 5.066(9)$, $c = 24.993(3)$	555.6
$CeNi_3$	$P6_3/mmc$	$a = 4.958(9)$, $c = 16.515(1)$	351.7
LaY_2Ni_9	$R-3m$	$a = 5.034(2)$, $c = 24.507(1)$	537.9
CeY_2Ni_9	$R-3m$	$a = 4.986(1)$, $c = 24.658(1)$	530.9

mented in FULLPROF program. The unit cell parameters for each sample are summarized in Table 1. The values obtained here agree well with those reported previously [4,8].

2.2. Solid-H_2 reaction

Prior to solid-H_2 reaction, the samples were mechanically ground into 38 μm powder and loaded into stainless steel reactors in a nitrogen-filled glove box. The reactors were then connected to the Sievert's apparatus. Fifteen cycles were performed between 5.5 MPa H_2 pressure and vacuum at 25 °C and 200 °C, respectively. The resulting phase components were identified by XRD.

2.3. Electrochemical measurements

The electrochemical measurements were conducted in a three-compartment cell at 30 °C. The electrolyte was 6 M KOH solution. The working electrode was made by mixing the sample powder with carbonyl Ni powder in a weight ratio of 1:4. The mixture was then cold-pressed into a pellet (10 mm in diameter) under 16 MPa pressure. $NiOOH/Ni(OH)_2$ was used as counter electrode, and Hg/HgO as reference electrode. In each cycle, the electrode was charged at 50 mA g^{-1} for 8 h followed by a 10 min rest, and then discharged at 30 mA g^{-1} until reaching the cut-off voltage of −0.6 V versus Hg/HgO.

3. Results

3.1. Phase transition after solid-H_2 reaction

XRD patterns of the four samples before and after absorption/desorption cycling under various conditions are shown, respectively in Figs. 1–4. In general, it can be said that all compounds showed partial amorphous nature, i.e. HIA, to some extent. This is evidenced from the disappearance of some Bragg peaks, the peak broadening, the remarkable increase in background and the significant decrease in diffraction intensities.

For $LaNi_3$ cycled at 25 °C, some new and broad Bragg peaks evolved in the range of 25–50°, see Fig. 1(b), and approximately matched to those of $LaNi_5$. This became more evident when the temperature was raised to 200 °C, the diffraction peaks from the $LaNi_5$ can be clearly identified, see Fig. 1(c) and (d). Besides, the formation of LaH_2 was also observed. These results are not the same as reported by Chen et al. showing that $LaNi_3$ decomposes totally to amorphous phase upon hydrogenation [4]. Moreover,

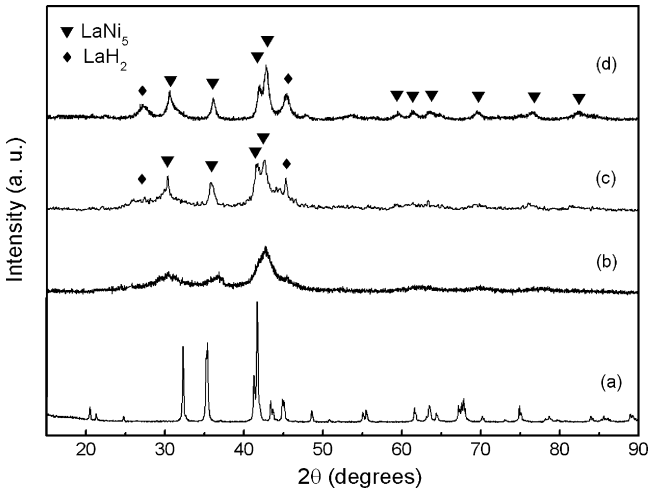

Fig. 1. XRD patterns of $LaNi_3$ cycled under 5.5 MPa H_2. The initial sample (a), cycled for 15 times at 25 °C (b), cycled for once (c) and 15 times (d) at 200 °C. For the sake of comparison in the same figure, the intensities of (b)–(d) are enhanced by five times.

it can be seen from Fig. 1(c) that HIA and other phase changes occurred immediately once $LaNi_3$ absorbed H_2 for the first time.

For $CeNi_3$, LaY_2Ni_9 and CeY_2Ni_9, it can be seen from Figs. 2(b)–4(b) that after cycled at 25 °C, the initial Bragg peaks were replaced by some weak and broad ones. These broad peaks are located around the same positions than those observed for the samples cycled at 200 °C, which were more evident and could be identified to those of RNi_3 and RNi_5. In addition, unlike the case of $LaNi_3$, the formation of binary hydrides, such as RH_x or YH_x, was not observed in the cases of CeY_2Ni_9 and LaY_2Ni_9, even at 200 °C.

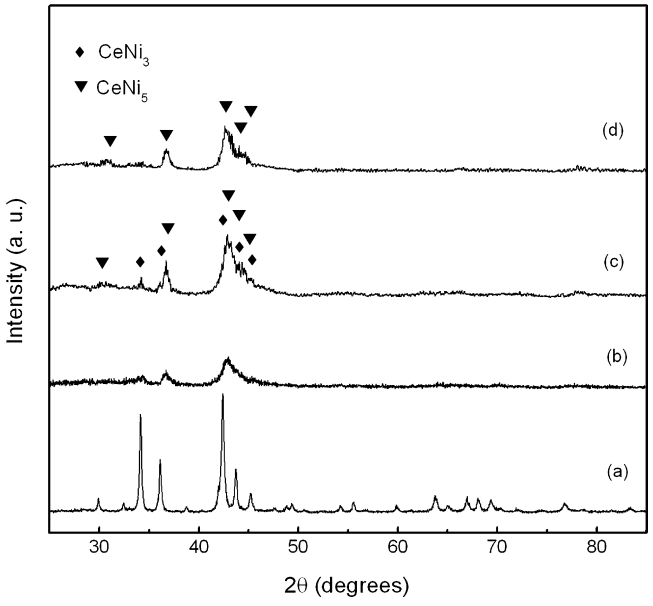

Fig. 2. XRD patterns of $CeNi_3$ cycled under 5.5 MPa H_2. The initial sample (a), cycled for 15 times at 25 °C (b), cycled for three times (c) and 15 times (d) at 200 °C. For the sake of comparison in the same figure, the intensities of (b)–(d) are enhanced by five times.

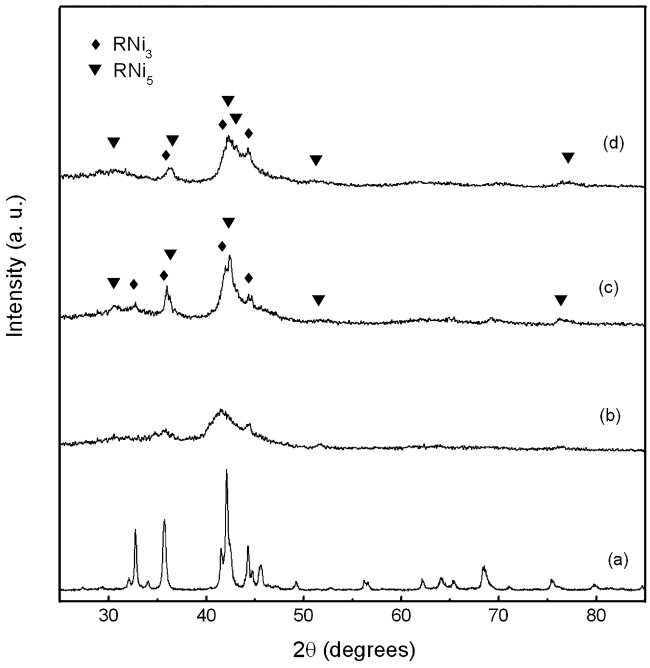

Fig. 3. XRD patterns of LaY_2Ni_9 cycled under 5.5 MPa H_2. The initial sample (a), cycled for 15 times at 25 °C (b), cycled for three times (c) and 15 times (d) at 200 °C. For the sake of comparison in the same figure, the intensities of (b)–(d) are enhanced by five times.

3.2. Electrochemical measurements

Fig. 5(a)–(d) depicts the evolution of the discharge curves with cycle number for $LaNi_3$, $CeNi_3$, LaY_2Ni_9 and CeY_2Ni_9. One can note that the discharge curves for each compound are discontinuous at around the potential of −0.75 V, indicating that more than one discharge process is involved. The discharge capacity as a function of cycling number is shown in Fig. 6. It can be seen that, for La samples, the maximum capacity was reached after three cycles, with 175 and 260 mA g^{-1} for $LaNi_3$ and LaY_2Ni_9, respectively whereas for $CeNi_3$ and CeY_2Ni_9, the capacities start from 240 and 205 mA g^{-1}, respectively and decrease continuously with the increase of cycling number. The capacity loss after 20 cycles was 16%, 42%, 61% and 59% for $LaNi_3$, LaY_2Ni_9, $CeNi_3$ and CeY_2Ni_9, respectively.

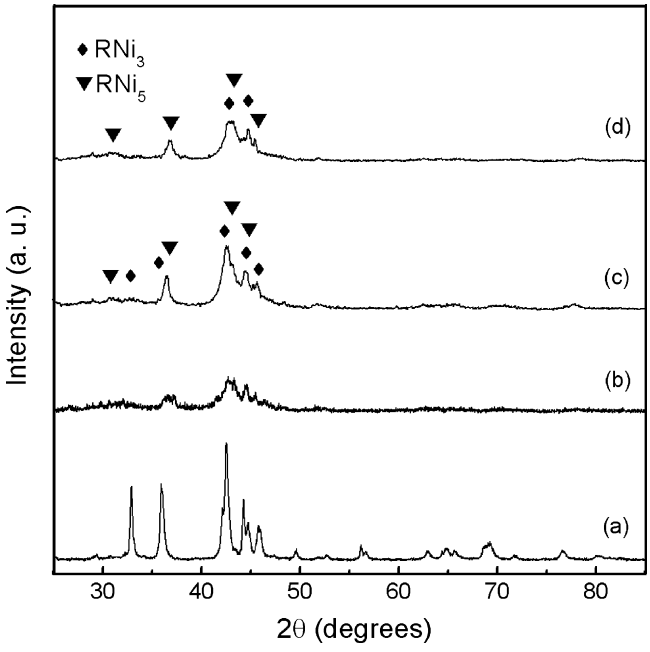

Fig. 4. XRD patterns of CeY_2Ni_9 cycled under 5.5 MPa H_2. The initial sample (a), cycled for 15 times at 25 °C (b), cycled for three times (c) and 15 times (d) at 200 °C. For the sake of comparison in the same figure, the intensities of (b)–(d) are enhanced by five times.

4. Discussion

The RM_3 structures contains a long-range stacking arrangement of which one-third is RM_5 and two-thirds RM_2 [2], therefore, the hydrogen storage properties of RM_3 could be regarded as the combination from both the RM_5 and RM_2 subunits. It is already known that RM_5 compounds maintain crystalline structures after hydrogen absorption, while RM_2 C15 Laves compounds decompose readily to amorphous phases [9–14]. Taking these facts into consideration, it is reasonable to deduce that the amorphization occurring in RNi_3 compounds is probably caused by the RNi_2 subunits.

For $LaNi_3$, the hydrogen absorption by its $LaNi_2$ subunits induces the local lattice to become a disorderly one, leading to the formation of amorphous phase. At the same time, the $LaNi_5H_x$ crystallites formed by the $LaNi_5$ subunit start to precipitate. If the temperature is high enough, such as at 200 °C in the present study, $LaNi_2H_x$ may disproportionate to form LaH_2, and the left Ni-rich $LaNi_2$ subunits thus transforms into $LaNi_5$. Combining these with the XRD results of Fig. 1, we may describe what happened in the $LaNi_3$ by:

$$3LaNi_3 \xrightarrow{H_2,25\,^\circ C} 2LaNi_2H_x(\text{amorphous}) + LaNi_5H_y$$

$$LaNi_2H_x(\text{amorphous}) \xrightarrow{H_2,200\,^\circ C} (3/5)LaH_2 + (2/5)LaNi_5H_z$$

As a support for the above, the precipitation of LaH_2 and $LaNi_5H_z$ from $LaNi_2H_x$ was indeed observed by Chung and Lee [14]. Note that the LaH_2 was not found at 25 °C, see Fig. 1(b), which suggests that the onset decomposition temperature for the amorphous $LaNi_2H_x$ is higher than 25 °C. For $CeNi_3$, CeY_2Ni_9 and LaY_2Ni_9, similar processes may occur during cycling. According to the XRD patterns of the samples cycled at 200 °C in Figs. 2–4, some peaks from the RNi_3 phase still remained after three cycles, indicating that HIA and other phase transitions are slower in these three compounds than in $LaNi_3$. In terms of the studies by Aoki et al. [12], HIA in C15 Laves RM_2 compounds is strongly dependent on the atomic size ratio between r_R and r_M, and $r_R/r_M > 1.37$ is a critical value for HIA occurring. Applying this theory to the $LaNi_3$, $CeNi_3$, CeY_2Ni_9 and LaY_2Ni_9, the value of r_{La}/r_{Ni}, r_{Ce}/r_{Ni} and r_Y/r_{Ni} is 1.50, 1.48 and 1.42, respectively, therefore, one may predict that the tendency to HIA should be in the order $LaNi_2 > CeNi_2 > YNi_2$. This is consistent with the results observed above that HIA occurred immediately in $LaNi_3$ and proceeded gradually in $CeNi_3$, LaY_2Ni_9 and CeY_2Ni_9.

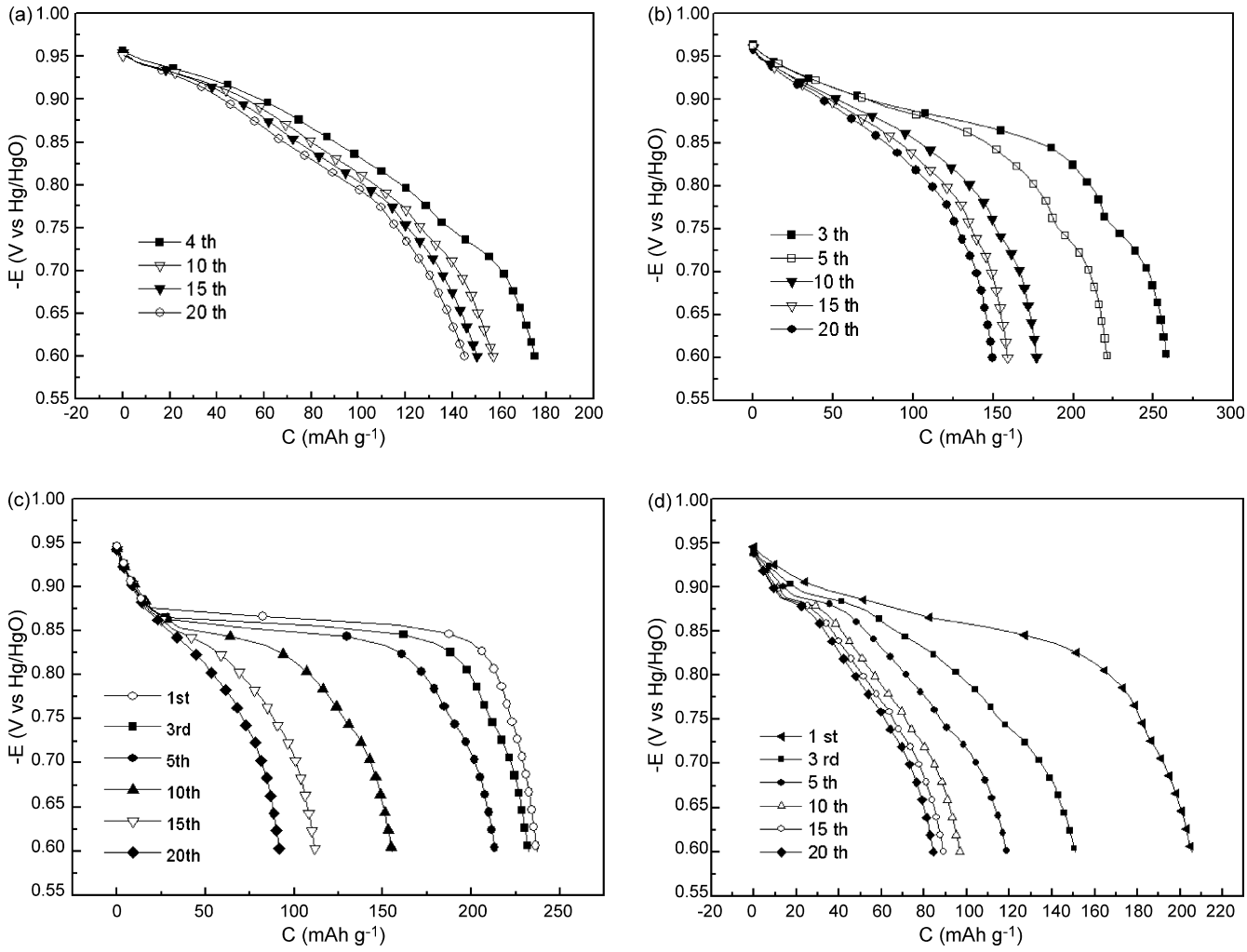

Fig. 5. Evolution of discharge curves with cycle number for $LaNi_3$ (a), LaY_2Ni_9 (b), $CeNi_3$ (c) and CeY_2Ni_9 (d).

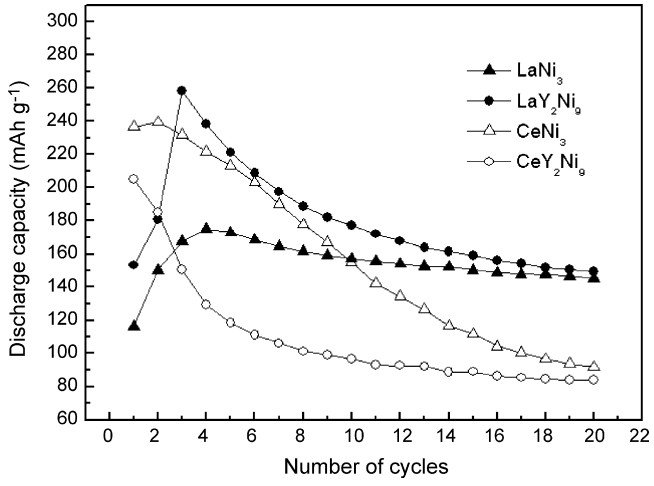

Fig. 6. Discharge capacity as a function of cycling number for $LaNi_3$, $CeNi_3$, LaY_2Ni_9 and CeY_2Ni_9.

The phase transition processes are further supported by the electrochemical measurements from four aspects. First, as shown in Fig. 6, compared to the LaY_2Ni_9, $CeNi_3$ and CeY_2Ni_9 samples, the maximum capacity for $LaNi_3$ is the lowest, but remained constant over 20 cycles. This can be understood by the results of the solid-H_2 reaction obtained at 25 °C, i.e. most of the $LaNi_3$ transform into irreversibly amorphous phase immediately after absorption, while HIA occurs slowly in LaY_2Ni_9, $CeNi_3$ and CeY_2Ni_9, the higher capacities are thus obtained in the first three cycling. Second, the HIA processes can also be deduced from the evolution of the discharge curves in Fig. 5. For the $LaNi_3$, almost no plateau is observed in the discharge curves from the first to the 20th cycle. For the other three samples, however, a plateau is clearly visible in the first five cycles (though it disappears as the cycle number increases). This difference suggests that under the same conditions of charging, the amounts of crystalline hydride decreases faster in $LaNi_3$ than in LaY_2Ni_9, $CeNi_3$ and CeY_2Ni_9. Third, the second discharge process started at around −0.75 V corresponds to some irreversible processes that are responsible for the loss of capacity with cycling. These irreversible processes may associate with the formation of highly stable binary hydrides and amorphous

phases, as evidenced by the XRD results in solid-H_2 reaction. Finally, it should be noted that although the initial capacities are different for the first few cycles (see Fig. 6), the two La-containing samples or the two Ce-containing samples end with almost the same capacities after 20 cycles, i.e. about 145 mA g^{-1} for $LaNi_3$ and LaY_2Ni_9, and 85 mA g^{-1} for $CeNi_3$ and CeY_2Ni_9. This feature suggests strongly that after 20 cycles, the final active phases are the same in each case. According to XRD results in solid-H_2 reaction, we believe that this final active phase is associated with RNi_5-related one. The most likely outcome is the $LaNi_5$ for $LaNi_3$ and LaY_2Ni_9, and the $CeNi_5$ for $CeNi_3$ and CeY_2Ni_9, if considering that the La(Ce)Ni_2 and YNi_2 are no longer active after decomposition. In situ XRD study on these compounds under electrochemical condition will provide more accurate information, which is in progress.

5. Conclusions

Both solid-H_2 reaction and electrochemical measurements were conducted to examine the structure stability of RNi_3 and RY_2Ni_9 (R = La, Ce) compounds during hydrogen absorption/desorption cycles. It is found that all compounds suffered from partial HIA to some extent, depending on the RNi_2 subunits in their crystal structures. HIA occurred more quickly in $LaNi_3$ than in $CeNi_3$, LaY_2Ni_9, and CeY_2Ni_9. These observations were confirmed by the electrochemical measurements: in the first few cycles $LaNi_3$ showed much lower capacity than the other three compounds; in the following cycles, the capacity of $LaNi_3$ was relatively stable while those of $CeNi_3$, LaY_2Ni_9 and CeY_2Ni_9 decreased gradually. Besides HIA, the precipitation of RNi_5 was found in the cycled RNi_3 and RY_2Ni_9 (R = La, Ce) compounds.

Acknowledgement

This joint project was financially supported by a grant (no. 045207034) from the Science and Technology Committee of Shanghai Municipality.

References

[1] D.T. Cromer, C.E. Olsen, Acta Crystallogr. 12 (1959) 689–694.
[2] B.D. Dunlap, P.J. Viccaro, G.K. Shenoy, J. Less-Common Met. 74 (1980) 75–79.
[3] D.M. Kim, K.J. Jang, J.Y. Lee, J. Alloys Compd. 293–295 (1999) 583–592.
[4] J. Chen, H.T. Takeshita, H. Tanaka, N. Kuriyama, T. Sakai, I. Uehara, M. Haruta, J. Alloys Compd. 302 (1–2) (2000) 304–313.
[5] J. Chen, N. Kuriyama, H.T. Takeshita, H. Tanaka, T. Sakai, M. Haruta, Electrochem. Solid-State Lett. 3 (2000) 249–252.
[6] A. Maeland, A. Andersen, K. Videm, J. Less-Common Met. 45 (1976) 347–350.
[7] R. Baddour-Hadjean, L. Meyer, J.P. Pereira-Ramos, M. Latroche, A. Percheron-Guégan, Electrochem. Acta 46 (15) (2001) 2385–2393.
[8] M. Latroche, A. Percheron-Guégan, J. Alloys Compd. 356–357 (2003) 461–468.
[9] H.-W. Li, K. Ishikawa, K. Aoki, J. Alloys Compd. 399 (2005) 69–77.
[10] K. Aoki, T. Yamamoto, T. Masumoto, Scripta Metall. 21 (1987) 27–31.
[11] M. Dilixiati, K. Kanda, K. Ishikawa, K. Aoki, J. Alloys Compd. 337 (2002) 128–135.
[12] K. Aoki, X.-G. Li, T. Masumoto, Acta Metall. Mater. 40 (7) (1992) 1717–1726.
[13] V. Paul-Boncour, C. Lartigue, A. Percheron-Guégan, J.C. Achard, J. Pannetier, J. Less-Common Met. 143 (1988) 301–313.
[14] U.I. Chung, J.Y. Lee, J. Non-Crystal. Solids 110 (1989) 203–210.